Coastal methane emissions triggered by ship passages

communications earth & environment

Article

A Nature Portfolio journal

https://doi.org/10.1038/s43247-025-02344-8

Coastal methane emissions triggered by ship passages

Amanda T. Nylund [1,2] ✉, Johan Mellqvist [3], Vladimir Conde [3], Kent Salo [1,3], Rickard Bensow [1], Lars Arneborg [2], Jukka-Pekka Jalkanen[4], Anders Tengberg [1] & Ida-Maja Hassellöv [1] ✉

Estuarine and coastal areas are important sources of methane emitted to the atmosphere through diffusion or ebullition. These processes can be triggered by pressure changes and water column mixing, which can be induced by ships. However, the contribution of ship-triggered emissions is unknown and missing in current emission inventories. Here we show evidence of extensive ship-induced methane emissions and an estimated methane flux (11.1 mmol m^{-2} day^{-1}) from Neva Bay shipping lane. The flux is 10–1000 times higher than reported global estuarine/coastal fluxes, and of similar magnitude as aquatic methane emission hotspots. Our results indicate that ship-induced pressure changes (30–60 mbar) trigger methane emission, comparable with observed emissions induced by tidal pressure changes. The ship-triggered methane emissions corresponded to a 22% increase of emitted carbon dioxide equivalents, compared to the combustion related exhausts. Our results demonstrate the need to include shipping lanes when assessing estuarine/coastal methane emissions.

Methane (CH_4) is the second most important greenhouse gas when it comes to climate forcing, and understanding the processes governing CH_4 emissions is necessary to assess and mitigate global warming[1,2]. Recent estimates of the global CH_4 budget allocate 50–65% of the global CH_4 emissions to anthropogenic sources[1] and 35–41% to aquatic systems. Marine CH_4 emissions comprise 3.2–7.7%[3] of the aquatic sources, dominated by shallow coastal areas and estuaries[4,5], where ship traffic often is intense[6,7] (Supplementary Fig. 1). Shipping is one anthropogenic source of atmospheric CH_4 emissions, from fuel combustion and methane slip from engines using Liquified Natural Gas (LNG)[8–10]. In addition, ship induced waves have been reported to cause pressure changes triggering emissions of CH_4 from natural sources[11,12].

In coastal areas, CH_4 is emitted to the atmosphere via ebullition and/or diffusive gas transfer[5]. Ebullition events often occur in a limited time and space, which is why they can be difficult to capture during field sampling, leading to underestimated total CH_4 emission from the investigated area[12–16]. Moreover, ebullition is not accurately measured from water samples of dissolved CH_4[17], but requires methods capturing CH_4 present in gas bubbles, such as floating chambers[12,18], eddy covariance (EC) measurements[16], or acoustic observations of bubbles[13,15,16]. Diffusive emission to the atmosphere occurs when the theoretical water concentration in equilibrium with the air partial pressure is smaller than the actual water concentration, and is governed by the magnitude of this concentration difference and the turbulence intensity just below the surface[19,20]. Large bubbles increase air-sea gas transfer[21,22] and water depth and stratification affect the rate and efficiency of CH_4 gas transfer from the sediment to the atmosphere[14,23–26]. Finally, a decrease in pressure can affect both diffusive gas transfer and trigger ebullition events[11–13,15,27–29].

Ships can impact the hydrodynamic pressure at the sea floor, through waves or by the squat effect[30] (a pressure reduction below the hull in shallow water). Moreover, shipping can introduce large bubbles in the water column[31,32] and impact water column stratification[31–34], and turbulence intensity at the surface[33,34]. Hence, ships can trigger ebullition events, induce pore water pumping, and increase diffusive gas transfer and bubble ascent. The co-occurrence of intense ship traffic and areas with high CH_4 flux (Supplementary Fig. 1), indicates that ship-induced CH_4 emissions could be an important process, requiring further investigation.

At water depths <10 m, a majority of the CH_4 emitted from the sediment as bubbles will reach the atmosphere[5,14]. In water depths >10 m, the air-sea flux rate of CH_4 is higher in a well-mixed water mass compared to a stratified water mass[23–26,35,36]. Turbulent ship wakes often exceed 10 m depth, frequently reaching depths >18 m[33,34]. Hence, ship-induced vertical mixing could play a role in increasing the air-sea CH_4 flux in areas with intense ship traffic. CH_4 ebullition events induced by bottom pressure-drop have been

[1]Department of Mechanics and Maritime Sciences, Chalmers University of Technology, Hörsalsvägen 7A, SE 412 58 Göteborg, Sweden. [2]Swedish Meteorological and Hydrological Institute (SMHI), Göteborgseskaderns Plats 3, SE 426 71 Västra Frölunda, Sweden. [3]Department of Space, Earth and Environment, Chalmers University of Technology, Hörsalsvägen 11, SE 412 58 Göteborg, Sweden. [4]Finnish Meteorological Institute, Erik Palmenin aukio 1, FI-00560 Helsinki, Finland. ✉e-mail: amanda.nylund@smhi.se; ida-maja@chalmers.se

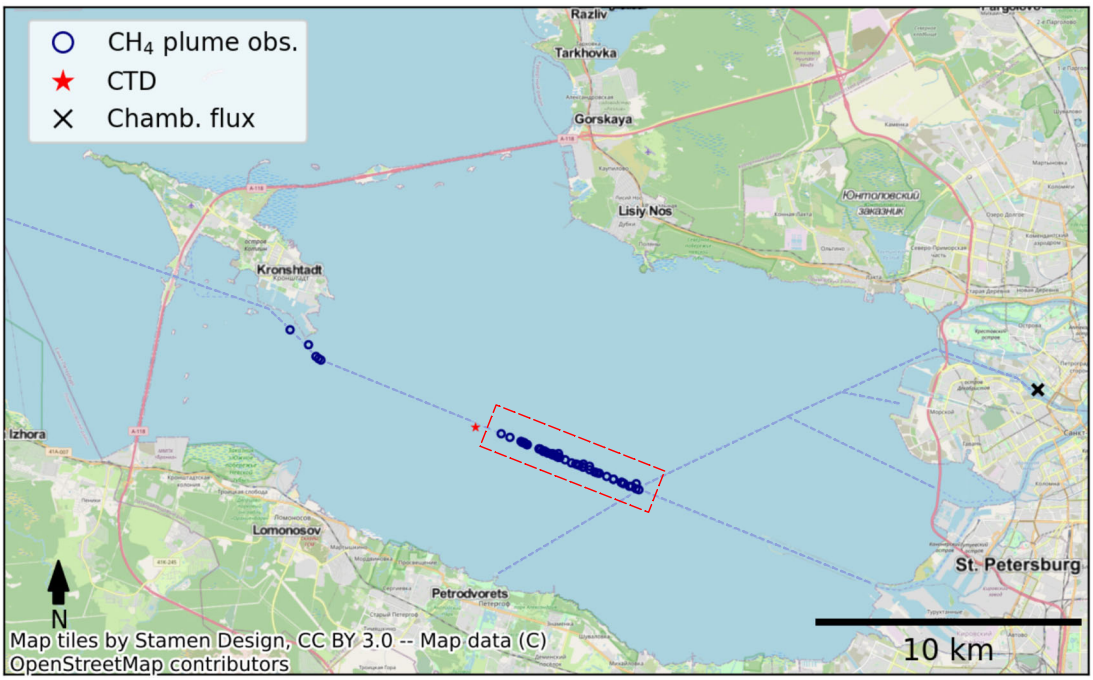

Fig. 1 | Map over the Neva Bay sampling area. Shipping lanes are indicated by dashed blue lines and clear CH_4 plume observations by dark blue circles. The sampled section estimated to 5.46 km long and 0.12 km wide (0.66 km^2), is indicated by the red dashed box. The location of the CTD profile is indicated by the red star and the chamber flux measurements by the black cross. The flood protective dam enclosing the west side of the bay is indicated by the red line (road) crossing from the south shore to the Kotlin island and over to the north shore.

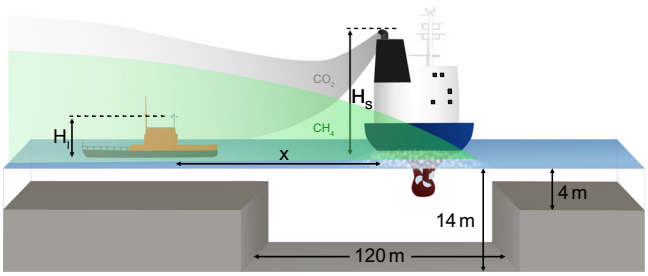

Fig. 2 | Field work setup for the emission measurements in the shipping lane channel. Note that the illustration is not true to scale. The smokestack from the ship chimney is indicated as a grey plume and the methane emission in the ship wake as a green plume. The inlet for the gas measurements was located on top of the sampling vessel (orange ship) at 6.5 m (2011) and 8.5 m (2012) height (H_I). The water depth and dimension of the channel are indicated, as well as the distance between the instrument and the ship (x). The ship height above water (H_S) was estimated as the keel to mast height minus the ship draught.

observed in relation to water level changes from tides[15,37,38] and wind-induced surface waves[13], as well as weather related drops in atmospheric pressure[27]. Further, pressure drop caused by the passing of ship-induced surface waves, have been observed to trigger ebullition events[12] and pore water pumping[11]. Consequently, we hypothesize that the largest impact from shipping on air-sea CH_4 flux is through ship-induced pressure drops triggering ebullition events. Acknowledging all ships to have the potential to cause CH_4 emission is, to the best of our knowledge, a novel approach compared to previous considerations limited to the use and combustion of carbon-based fuels[8–10].

The aim of this study is to quantify ship-induced CH_4 emission in a highly trafficked CH_4-rich estuarine area and to compare its relative importance to other ship-related and natural CH_4 emissions. To investigate the physical factors governing the occurrence and magnitude of ship-induced CH_4 flux, we used Detached Eddy Simulation (DES) Computational Fluid Dynamics (CFD) modelling in full-scale, to study the turbulent ship wake and ship-induced pressure field of two ships. Two field campaigns were conducted in the Neva Bay, Russia (2011 and 2012) (Fig. 1), where a Picarro CRDS (cavity ring-down spectrometer) was used to measure carbon dioxide (CO_2) and CH_4 plumes from passing ships[39,40] (see "Methods" and Fig. 2). The known dispersion of the CO_2 plume, calculated from modelled values of fuel consumption from the Ship Traffic Emission Assessment Model (STEAM) model[41], was used to estimate the emission of CH_4, assuming a similar dispersion of the CO_2 and CH_4 plume ("Methods" and SI Methods). For comparison, the natural CH_4 flux in the Neva Bay estuary was measured with a floating flux chamber connected to the CRDS instrument, in a sheltered part of the Neva River mouth (Fig. 1). The Neva Bay shipping lane is intensively trafficked by a large variety of ships[42], and the water CH_4 concentration is high[43], providing a suitable field location to observe ship-induced CH_4 emissions. As a majority of the world's largest ports[44] are located in similar shallow estuarine environments (Supplementary Fig. 1), where sediment CH_4 production has been observed[23,24,45,46] (SI Table 1), the results presented in this study have implications for ports and intensively trafficked areas worldwide.

Results

Observed ship-triggered CH_4 emissions

In the field observations 464 ship plumes were detected, of which 220 (47%) fulfilled the data quality inclusion criteria in the emission analysis (see "Methods"). Of the analysed passages 28% had a significant CH_4 emission (plume). Although delayed (44 ± 36 s), the CH_4 emission generally had a similar shape (Supplementary Fig. 2) and length compared to the CO_2 plume (length 125 ± 77 s and 105 ± 36 s, for CH_4 and CO_2 respectively) (all values presented are medians and all uncertainties ± one standard deviation (SD), unless otherwise specified). In 2012, the shipping lane was weakly thermally stratified at 1 m, with a uniform salinity ~0.051 [psu] and an oxygen saturation between 80 and 90% (Supplementary Fig. 3).

Ship type specific CH_4 emissions (E_{CH_4}) g s^{-1} are presented in Fig. 3. Container and cruise ships had the largest and highest number of CH_4 emission observations, as well as the highest percentage of passages inducing emissions (77% and 76%, respectively) (Table 1). The two largest CH_4

Table 1 | Emission and vessel specifications per ship type

Ship type	Nr. total plumes	Nr. CH_4 plumes	% CH_4 plumes	CH_4 [g s^{-1}]	Length [m]	Draught [m]	Width [m]	Speed [kts]	Power [kW]	ΔP [mbar]
Bulk	7	4	57%	3.56	175	10.1	28.5	11.1	3345	83.2
Cargo	74	4	5%	0.72	104	3.1	15.7	8.15	514	4.9
Container	26	20	77%	11.34	169	9.7	25.2	11.3	4867	61.3
Cruise	17	13	76%	5.42	279	7.9	32.2	12.2	5985	76.4
Other	6	2	33%	5.23	94	5.0	22.7	12.5	3272	38.3
Reefer	8	1	13%	6.62	150	9.1	22.5	11.8	3033	54.8
Ro-Ro	12	4	33%	1.12	153	7.0	20.7	10.7	2343	29.4
RoPax	9	5	56%	11.82	164	6.9	29.0	11.7	7918	52.4
Tanker (L)	33	7	21%	3.17	155	10.2	24.8	10.5	2913	56.8
Tanker (S)	22	2	9%	1.57	133	3.3	16.9	8.0	680	6.1
Tug	5	0	0%							
Total	219	62	28%							

The number of total plumes, CH_4 plumes, the percentage of passages inducing a clear CH_4 emission, and the median CH_4 emission [g s^{-1}] for each ship type included in the emission analysis. The ship type specific median length [m], draught [m], width [m], speed [kts], power [kW], and calculated estimated pressure change (ΔP) [mbar], of the ships categorised as having a clear CH_4 plume. Ro-Ro stand for Roll on-Roll off cargo vessels, RoPax is Roll on Passenger vessels, Tanker (L) are tankers with a draught ≥5 m, and Tanker (S) are tankers with a draught <5 m. The other category included 1 crane ship (CH_4 plume), 1 research vessel, 1 dredger, 2 vehicles carrier (1 CH_4 plume), and 1 water tanker.

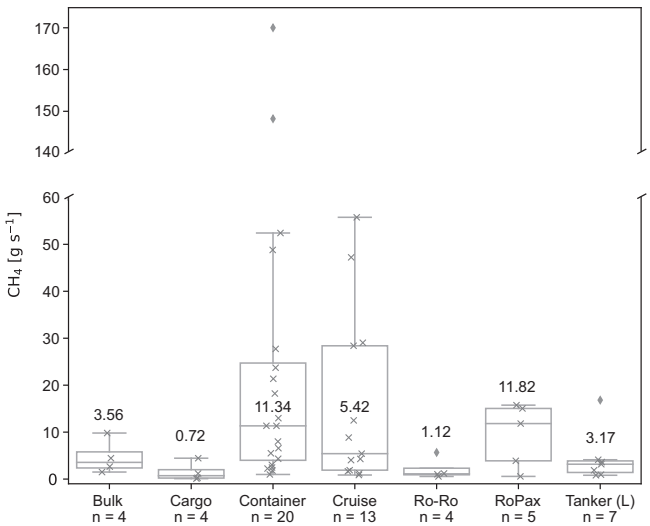

Fig. 3 | Observed CH_4 emissions per ship type. CH_4 emission [g s^{-1}] for the seven ship type categories which had more than three observed CH_4 plumes (see "Methods"). Note the broken y-axis for the two highest container observations. The number at each box indicate the median CH_4 emission, indicated by the horizontal line inside each box, the individual datapoints are denoted by grey x-symbols, and grey diamonds show outliers. The number of passages (n) for each ship type is indicated on the x-axis.

plumes, induced by container ships, were >10 times larger than the container ships' median value. Several CH_4 emissions of similar magnitude as the two container ship extremes, were present in the data not meeting the quality criteria (see "Methods"), indicating that these high values are extreme, but not unusual. Bulk and Roll on-Roll off passenger ships (RoPax) had comparatively high median emission and large share of passages inducing emission (57% and 56%, respectively).

The daily shipping lane CH_4 emission from the sampled section, estimated from a 24 h sampling period (see "Methods"), included 79 detected plumes of which 27% had a clear CH_4 plume. The total CH_4 emission and flux during the 24 h period was ~120 kg day^{-1} and 0.2 g m^{-2} day^{-1} (11 mmol m^{-2} day^{-1}), respectively, for the section of the shipping lane sampled during the campaign (Fig. 1). The increase in atmospheric CH_4 concentration (volume mixing ratio (VMR)) was below 0.5 ppm for 77% of the ship induced emissions and between 1.18 ppm and 4.77 ppm for the top 11% (7 passages). The diffusive sea-air CH_4 flux measured using the flux chamber in the Neva River mouth (Fig. 1), was ~0.5 mmol m^{-2} day^{-1}, i.e., around 20 times lower than the estimated shipping lane flux.

The average passage frequency was 3.1 ± 0.41 ships h^{-1} and the share of passages inducing emissions were 23 ± 5% (for frequency dataset, see "Methods"). The share of passages of each ship type was similar between the days. A high-resolution temporal analysis showed that during the time periods with no observed clear CH_4 plumes, there were few passages of the ship types frequently inducing CH_4 emissions (cruise and container) (Fig. 4).

Observed and modelled governing factors

CH_4 emissions of different magnitude were visible during a range of wind conditions (Supplementary Fig. 3). There was no correlation between ship-triggered CH_4 emission occurrence or intensity, with wind speed or direction. Higher wind speeds increase the background emission of CH_4 due to increased turbulence and diffusion[18,20], however, our ship-triggered emissions are calculated as emissions above background level (see "Methods"). Likewise, there was no trend linking the occurrence and magnitude of ship-triggered CH_4 emissions with air pressure or air temperature (Supplementary Fig. 4). Thus, our results indicate that the physical parameters governing the natural emission of CH_4, are not the main factors governing the likelihood or magnitude of ship-triggered CH_4 emissions.

Large ship-induced pressure changes (Δ*P*) correlated with the triggering (frequency) of CH_4 emissions, with a threshold value around ~60 mbar, above which all except two ships triggered a CH_4 emission (Fig. 5a). The two exceptions (orange data points > 60 mbar) had an elevation in CH_4, but the baseline concentration variations were too large for the observation to qualify as a Clear CH_4 emission (see "Methods"). A mixture modelling approach, integrating a logistic regression model and a log-normal regression model (see "Methods"), was used to investigate the relationship between CH_4 emissions and the calculated Δ*P* estimate, ship length, draught, and speed (Fig. 5). From the logistic regression model, odds ratios (ORs) quantifying the likelihood of clear CH_4 emissions relative to no emissions per specified unit increase, were calculated. The log-normal regression model was used to estimate how the magnitude of the CH_4 emission would increase (the fold change) for the same unit increases. A 20 mbar increase in pressure was associated with an OR of 4.37 (95% CI 2.99, 6.4) for triggering a clear emission (i.e. 4.37 increase in likelihood) and a 2.99-fold increase in CH_4 emission magnitude (95% CI 2.67, 3.34) (Fig. 5).

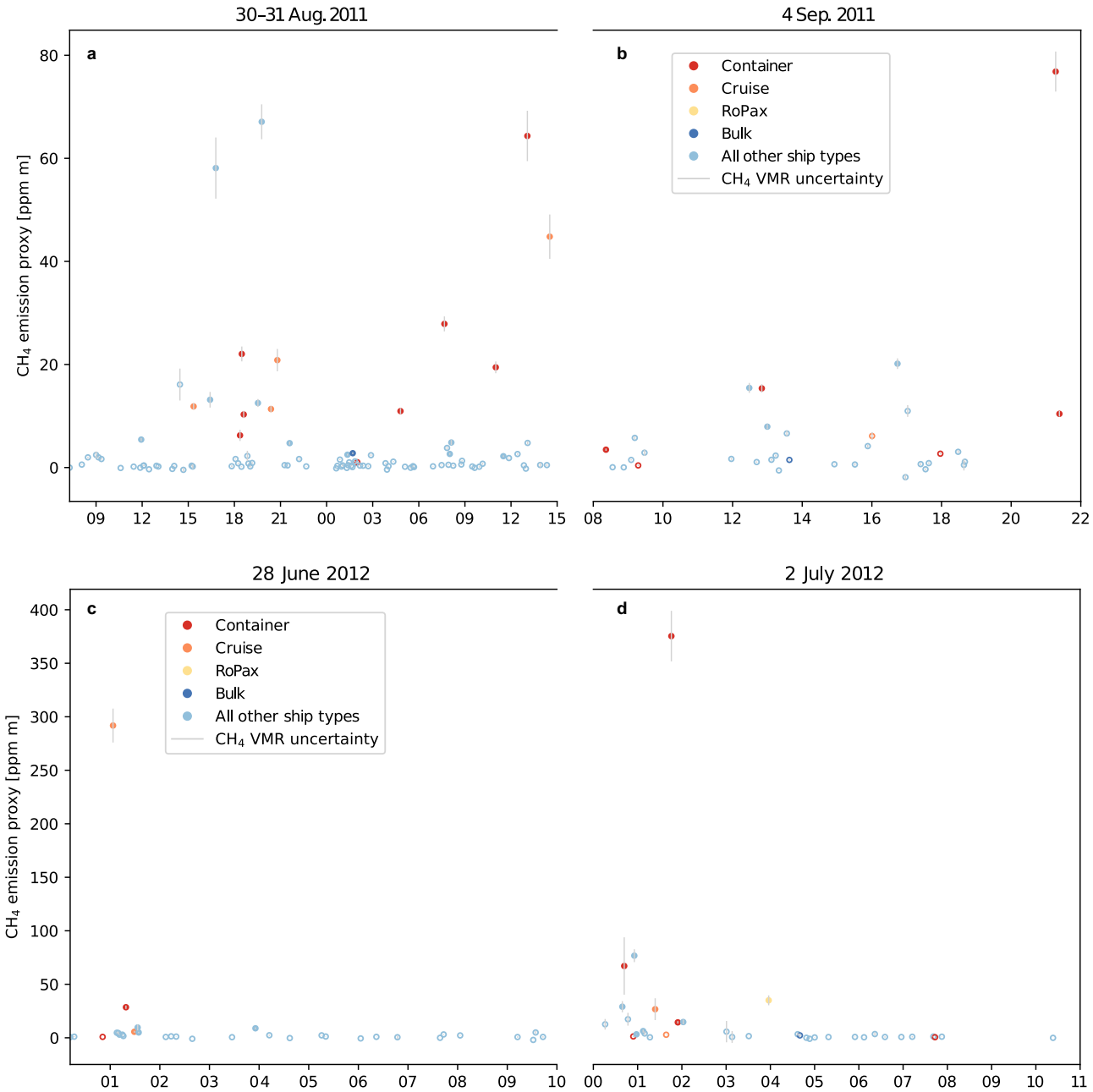

Fig. 4 | Temporal variation of observed methane emissions. Estimated CH_4 emission proxy (observed CH_4 plume area [ppm s] multiplied with the wind speed [m s^{-1}], see Supplementary Methods for details) for the 2011 and 2012 frequency dataset. (**a**) 30–31 August 2011, (**b**) 4 September 2011, (**c**) 28 June 2012, (**d**) 2 July 2012. The x-axis indicates the hour of the day. Circle colour indicates ship type, filled circles are clear CH_4 emissions and empty circles are no clear CH_4 emissions. Error bars indicate the total CH_4 plume area uncertainty (se Supplementary Eq. (4) in Supplementary Methods).

This is in line with the OR and fold-change calculated for the ship speed and size (Fig. 5), which is expected since these parameters affect the ship-induced pressure. In summary, the results from the mixture model indicate a clear relationship between increased ship-induced pressure and emission occurrence and magnitude, described by the equation in Fig. 5.

There were also clear indications of ship size and speed threshold values for the triggering of CH_4 emissions (Fig. 5b–d). Ships with lengths <125 m and draughts <5 m very seldom induced CH_4 emissions, ships with draughts >9 m frequently induced large CH_4 emissions, and ships >250 m long always induced CH_4 emissions (Fig. 5b–d). Similarly, Larger ship speed correlated with higher and more frequent CH_4 emissions, with the largest CH_4 emissions induced by ships with speeds >12 knots and very few emissions induced by ships with a speed <9 knots (Fig. 5d), indicating a potential speed threshold for emissions magnitude as well as frequency. In addition to the threshold values, the mixture model results showed a clear relationship between increased speed and size and the likelihood and magnitude of the CH_4 emissions. A 50 m increase in ship length corresponded to an OR of 5.41 (95% CI 3.15, 9.32) for clear emissions and a 2.39-fold change in CH_4 emissions (95% CI 2.06, 2.77) (Fig. 5). For ship draught, a 1 m increase resulted in an OR of 1.73 (95% CI 1.47, 2.03) and a 1.76-fold change in CH_4 emissions (95% CI 1.49, 2.08), and a 1 knot increase in speed was associated with an OR of 2.35 (95% CI 1.81, 3.06) for clear emissions and a 2.37-fold change in CH_4 emissions (95% CI 1.82, 3.09) (Fig. 5).

The CFD model results showed a large difference between the pressure change (ΔP) field below the tanker (15–30 mbar) and the RoPax (30–60 mbar) (Fig. 6). As the tanker corresponds to a ship not inducing CH_4 emissions, these results indicate that the ΔP threshold value for

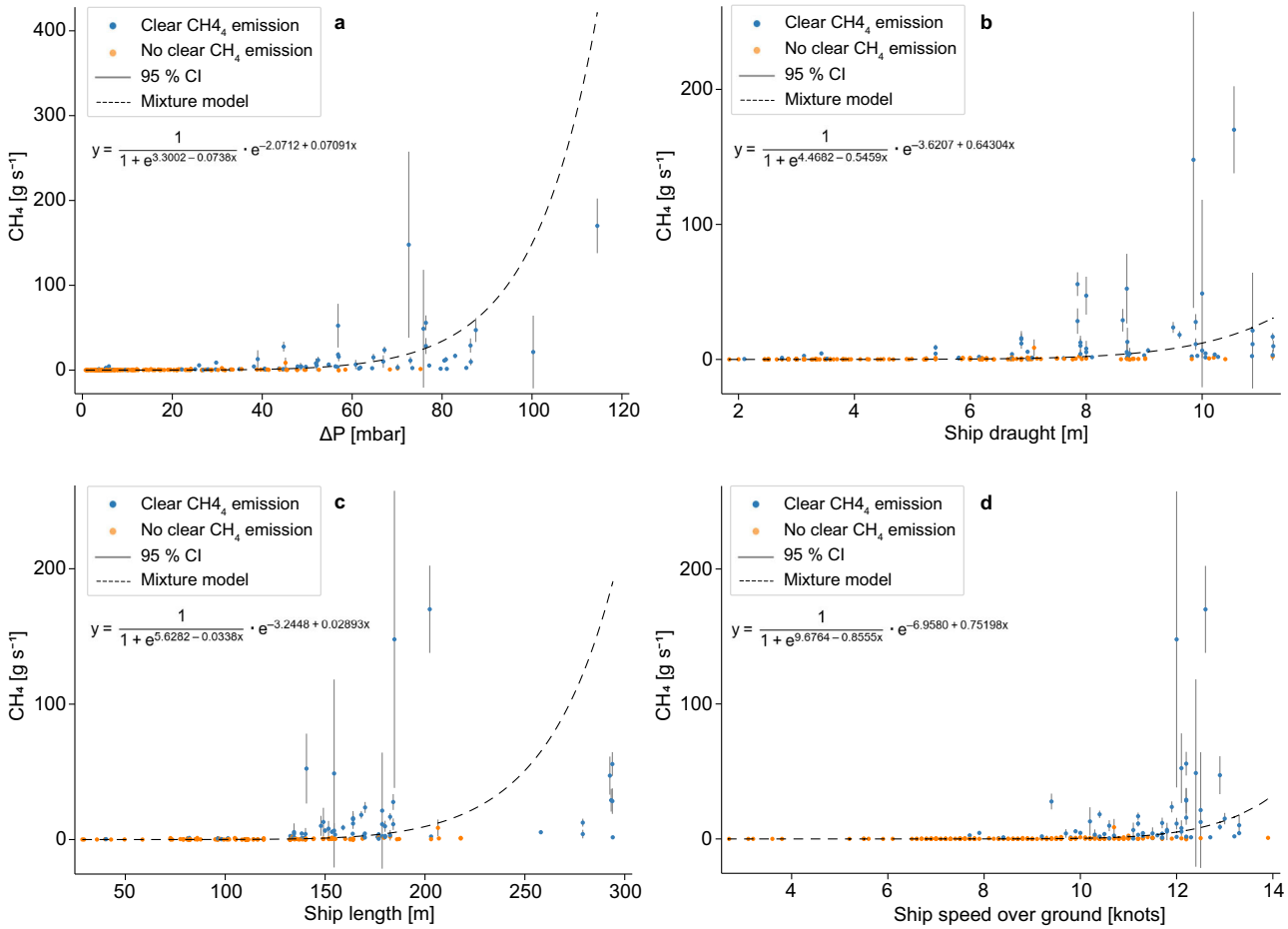

Fig. 5 | CH_4 emissions versus ship-induced pressure change, ship size, and ship speed. Association between CH_4 emission [g s^{-1}] and (**a**) the calculated estimate of the ship-induced pressure change (ΔP) [mbar], (**b**) ship draught [m], (**c**) ship length [m], and (**d**) ship speed over ground [knots]. The dashed line depicts the fitted mean trend, estimated using a logistic-log-normal mixture model (y). Blue dots indicate observations categorised as clear CH_4 emissions and orange dots are passages without clear CH_4 emissions. Error bars indicate the 95% confidence interval for the measurements (see Supplementary Methods for details).

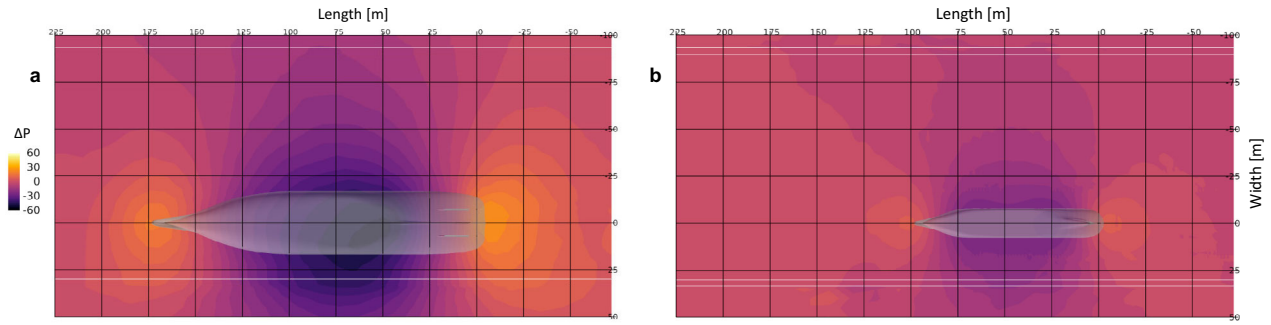

Fig. 6 | Modelled pressure change during ship passage. Pressure change (ΔP) in mbar, on the sea floor under the (**a**) RoPax and (**b**) tanker. The white horizontal lines indicate the shipping channel edges. The grid lines are placed every 25 m.

triggering a CH_4 emission lies between 30 and 60 mbar, in good agreement with our observations.

Discussion

The observed Neva Bay shipping lane CH_4 flux (11.14 mmol m^{-2} day^{-1}), is similar to reported fluxes from freshwater reservoirs and dams[47,48], lakes[47], estuarine mudflats[37,38], ebullition from CH_4 hotspot regions on the Arctic continental shelf[16], and in the upper range of observed fluxes in shallow coastal estuaries and bays around the Baltic Sea[14,49–51] (literature values in Supplemenatry Table 1). The average and lower range of the previously reported CH_4 fluxes for Baltic Sea estuarine and coastal areas[52–54] are 1–4 orders of magnitude lower than our observations. On a global scale, the estimated CH_4 flux from estuarine and coastal areas are ca 1–3 orders of magnitude lower than our observed flux[23,24,36,45,46,53,55] (Supplementary Table 1), for continental shelfs it is ca 2–4 orders of magnitude lower[46,51], and the order of magnitude is the same as for rivers, lakes, and wetlands[47], indicating that the Neva Bay shipping lane is a CH_4 flux hotspot.

The lower range Baltic Sea fluxes were mainly based on diffusive fluxes (Supplementary Table 1) and would miss any potential ebullition-driven emissions[17], whereas most of the upper range observations (Supplementary

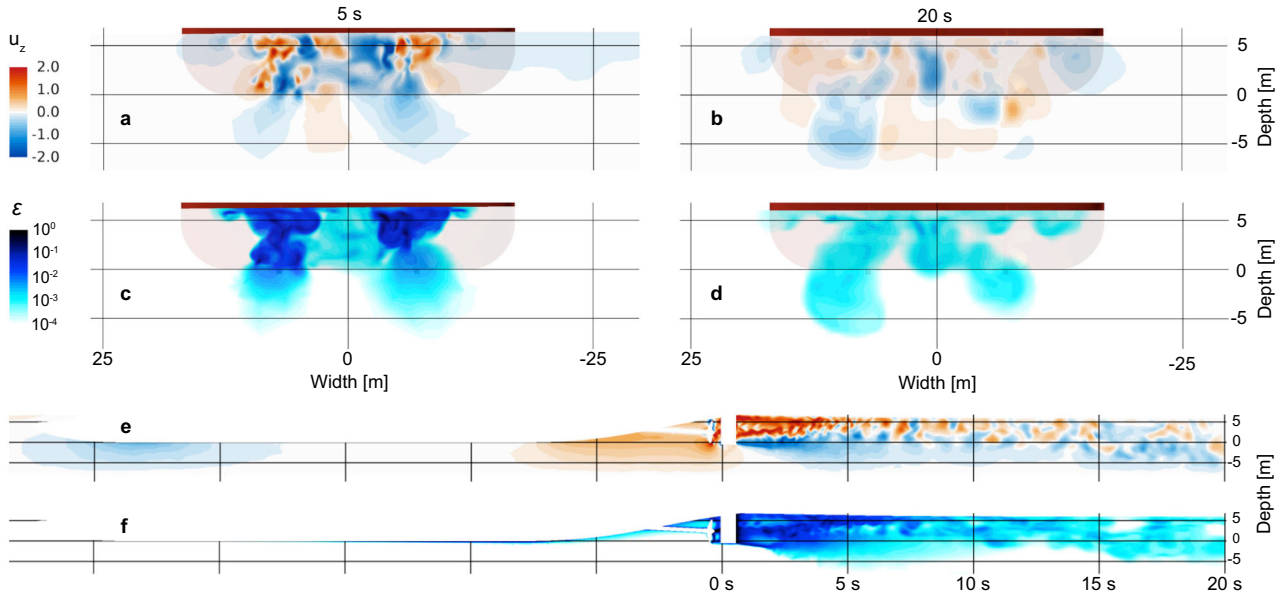

Fig. 7 | Modelled ship-induced vertical velocities (u_z) and turbulent kinetic energy dissipation rate (ε) in the RoPax wake. Vertical cross section of the modelled ship induced u_z in m s^{-1} (**a**, **b**) and ε in m^2 s^{-3} (**c**, **d**) over the wake width for the RoPax case, at 5 s (**a**, **c**) and 20 s aft the propeller (**b**, **d**). Vertical cross sections of u_z (**e**) and ε (**f**) during a ship passage, along the wake length from the bow to 20 s aft of the propeller. Water depth is 14 m and indicated on the y-axis as distance from the ship draught in metres.

Table 1) and our shipping lane estimate were of the total flux including ebullition. The Neva Bay CH_4 water concentration is high compared to other Baltic Sea areas[43,52], hence a high diffusive flux is expected, as indicated by the chamber flux measurements. Still, the observed chamber flux was 20 times lower than the estimated total shipping lane flux from the CRDS instrument observations. As the chamber measurement did not show presence of bubbles, it can be considered an estimate of the diffusive flux. Thus, the occurrence of ebullition events could be a potential explanation for the higher shipping lane flux, an hypothesis further supported by the observed relationship between ΔP and CH_4 emissions (Fig. 5), as pressure changes have been shown to trigger ebullition events[11–13,15,27,29].

The chamber flux measurement was made in a sheltered part of the Neva River, after attempts to measure close to the shipping lane failed due to waves. Although the shipping lane is more exposed and slightly deeper, we considered the locations comparable for getting an order of magnitude estimate of the shipping lane diffusive CH_4 flux, as both locations are within the Neva Bay estuary (Fig. 1) and have conditions favourable for methane production and release (shallow areas and a large input of riverine organic matter[14,56]). The highest previously reported summer CH_4 diffusive fluxes from estuarine and inshore areas in the Gulf of Finland have ranged between 1 and 2.8 mmol m^{-2} day^{-1}[14,50], and a global estimate for shallow shelf regions presented a flux of >0.03 mmol m^{-2} day^{-1}[5], placing our chamber measurement within one order of magnitude of previous estimates.

Our chamber measurement and previously reported fluxes can be used to estimate the relative contribution of the shipping lane area (3.276 km^2) to the total CH_4 emission of the entire Neva Bay area (400 km^2)[57]. With an ambient flux equal to our measured chamber flux (0.5 mmol m^{-2} day^{-1}), the shipping lane would contribute 15% of the total flux, and previously reported fluxes (0.03 and 2.8 mmol m^{-2} day^{-1})[5,14,50] give a rage of 3–77%. As the ambient flux estimate is based on diffusive fluxes, it is likely and underestimation. Nevertheless, the results indicate that ship-triggered emissions could be a substantial contributor to the total CH_4 emission in the Neva Bay area.

Our observed top 10% highest max peak CH_4 VMR in the flux dataset, ranged between 1.18–4.77 ppm. They are similar to concentration increases observed at Arctic continental shelf seep hotspots during ebullition (>1 ppm)[35], but ten times higher than storm-induced CH_4 flux increase in coastal Baltic Sea[49] and reported CH_4 slip peaks from LNG vessels[8].

Ship-induced pressure changes of 15–20 mbar have previously been observed[34], indicating that the modelled and calculated ΔP values are realistic. Tide-related pressure drops of ~20 mbar[29] have been shown to increase bubble release in a North Sea seepage area and tide-related pressure changes of 92 ± 120 mbar have been observed to trigger the onset of CH_4 flares in a >1200 m deep shelf slope seep[15]. Smaller changes in pressure can also trigger ebullition, and observations have shown an increase in ebullition of 18% per mbar drop in air pressure[27]. Consequently, the calculated ΔP of the observed vessels (0–120 mbar) (Fig. 5) and the modelled ΔP field range (15–60 mbar) (Fig. 6), were both of a magnitude shown to trigger and increase CH_4 emission. Air pressure changes during our field campaigns were of a magnitude that could influence the CH_4 emissions (~22 mbar), but there was no correlation with regards to emission magnitude or frequency (Supplementary Fig. 4).

Two of the largest ship types (container and cruise) triggered the most frequent and largest CH_4 emissions (Fig. 3, Table 1). However, mid-size RoPax vessels had the largest median emissions, whereas one of the biggest ship types (bulk) had the median. This suggests more complicated factors than the ship size governing the methane emissions. A potential explanation to the high values for the cruise and RoPax ship types, is their twin screw propeller configuration. The turbulent wake of two propellers affects a larger volume and area compared to a single propeller wake (Figs. 7, 8) and could lead to a more efficient outgassing and air-sea exchange. This is in line with observations[33,34] and modelling results of ships of similar size and type[34], which report a deeper and wider penetration of RoPax ship wakes compared to the smaller tanker. However, all container ships had single propellers, thus having two propellers is likely not the only parameter triggering CH_4 emissions. Consequently, our results indicate a complexity in the factors governing ship-induced CH_4 emissions, and that there might be additional ship type-specific parameters apart from speed, size, propeller configuration, and ΔP, which needs to be taken into consideration. The additional parameter of most interest is probably the hull shape (bulky or slender), as it affects the ship-induced pressure and ship resistance. The operation of the ship could also be of potential interest, as the way the ship is manoeuvred can affect the direction and intensity of the ship-induced turbulence.

Frequent outgassing of the sediments have been suggested to cause CH_4 depletion[11], requiring time to re-build the CH_4 concentration between ebullition events, but this is not supported by our results. On the contrary,

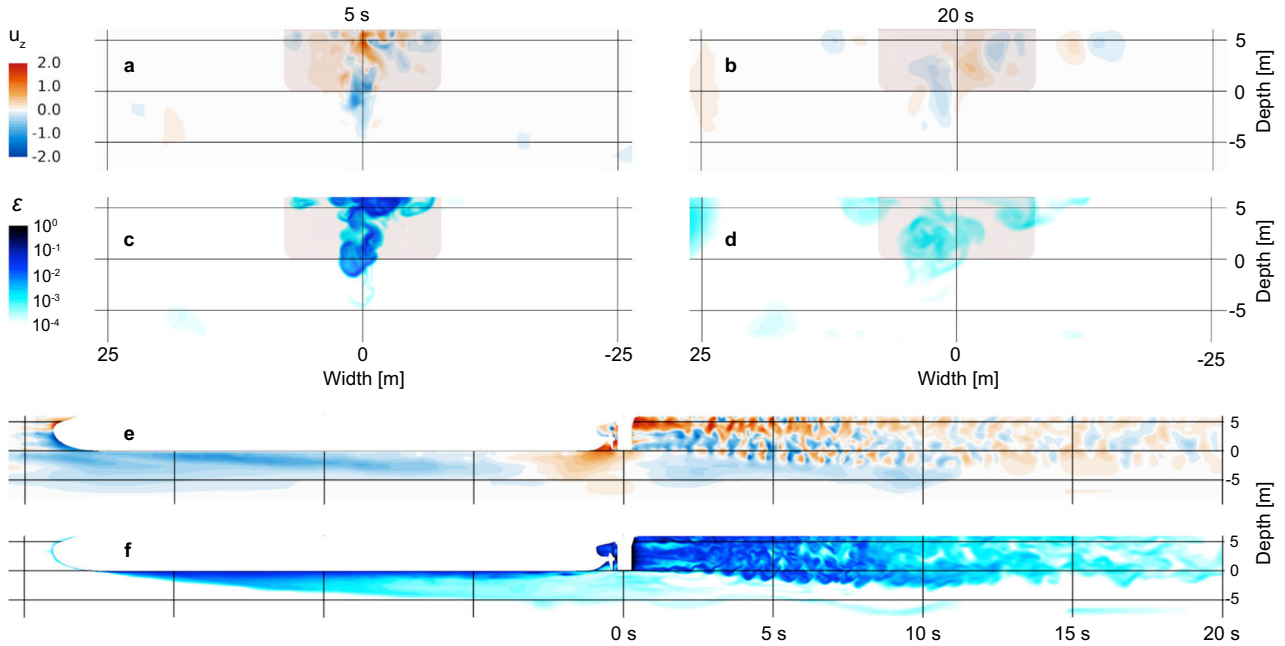

Fig. 8 | Modelled ship-induced vertical velocities (u_z) and turbulent kinetic energy dissipation rate (ε) and in the tanker wake. Vertical cross section of the modelled ship induced u_z in m s^{-1} (**a**, **b**) and ε in m^2 s^{-3} (**c**, **d**) over the wake width for the tanker case, at 5 s (**a**, **c**) and 20 s aft the propeller (**b**, **d**). Vertical cross sections of u_z (**e**) and ε (**f**) during a ship passage, along the wake length from the bow to 10 s aft of the vessel. Water depth is 14 m and indicated on the y-axis as distance from the ship draught in metres.

we frequently observed CH_4 emissions from successive ships, and the two largest emissions occurred within 25 min of a previous CH_4 emission (Supplementary Data 1), indicating that successive ship passages increase the likelihood of triggering emission. Our diverging results could be explained by differences in CH_4 production rate, as the previous study was conducted in an oligotrophic and well oxygenated lake, where CH_4 was limited to the sediment[11]. In contrast, the Neva Bay is eutrophic[57], has a high water CH_4 concentration[43] and ideal conditions for biogenic CH_4 production (see "Methods"), indicating that the CH_4 concentration and production rate is likely high enough to quickly re-build the CH_4 concentration between ship-triggered outgassing events. Alternatively, the environmental conditions favourable for CH_4 ebullition varies over time, and the timing of the ship passage is more important than the number of passages or type of ship. However, during the time periods in 2012 with few/no clear CH_4 emissions, there was only one passage of the ship types frequently inducing CH_4 emissions (Fig. 4). This indicates that the type of ship is a more important factor than the temporal variation in environmental conditions, but further studies are needed to fully resolve the factor(s) governing ship-triggered CH_4 emissions. Moreover, there were no observations of short and intensive CH_4 emission peaks between ship passages, which would be expected if natural ebullition was occurring, indicating that frequent event-type CH_4 emission only occur if ships are passing.

The modelling results show that the RoPax induces mixing in the entire water column (Figs. 7, 8), indicating that CH_4 at the sea floor would be brought to the surface by ship-induced mixing. This result is in agreement with previous field observations[33], where the median depth of ship-induced turbulence was 13 m, frequently reaching depths >18 m, and with a duration of 5–10 min after ship passage. Hence, with an average traffic of 2.3 ± 0.4 ships h^{-1}, the Neva Bay shipping lane would be under frequent influence of ship-induced mixing, and thus a well-mixed water mass. The bubbles in the turbulent wake[31,32] will further increase the air-sea gas flux. Consequently, ship-induced turbulence is likely increasing the diffusive CH_4 flux rate in the shipping lane. However, the respective contribution from increased diffusive flux and the triggering of ebullition events is yet to be established, but previous studies have shown that when ebullition occurs it exceeds the diffusive flux[12,47,48]. As our measurements were made above water, the results cannot be used to resolve the emission/ebullition processes in the sediment. Hence, future studies should include in situ pressure observations and underwater flux/ebullition estimates using acoustic instruments (i.e. an echosounder or sonar)[13,29,35]. However, near ship in situ observations in shipping lanes are challenging and needs to be further developed.

As biogenic CH_4 production increases with higher temperatures[14,23,28,48,54], our observations are representative for the summer period. Extrapolating our estimated daily total CH_4 emission from the Neva Bay shipping lane (117 kg d^{-1}) for the entire summer period (13 weeks), would give a total emission of CH_4 of 10.7 Mg. Using a conservative approach with a CH_4 conversion factor of 27 ± 11 over a 100 year time scale[58], the CH_4 emissions gives a greenhouse gas potential (GGP) of 0.29 ± 0.17 Gg CO_2 equivalents per summer or 3.2 ± 1.8 Mg d^{-1}. In comparison, a 20-year timescale and a conversion factor of 79.7 ± 25.8[58] gives 0.85 ± 0.39 Gg CO_2 equivalents or 9.3 ± 4.3 Mg d^{-1}. If the emissions are extrapolated to the entire Neva Bay shipping lane, the values will be five times higher (1.6 Gg). The daily variation in the occurrence and magnitude of ship-induced CH_4 emissions, makes this an uncertain estimate, but it gives an indication of the order of magnitude.

During a 24-h measurement period, the CH_4 emissions when passing the Neva Bay, on average corresponded to 22 ± 13% (100-year timescale) and 66 ± 30% (20-year timescale) of the CO_2 GGP from the ship's fuel combustion (14 Mg d^{-1}), for the ships triggering a clear CH_4 emission. The percentage varied between ship types, with large tankers having the highest percentage (35 ± 20%) and cruise vessels the lowest (18 ± 11%), on a 100-year timescale. Considering that these observations were made in 2011 and 2012, and the International Maritime Organisation (IMO) goal of peaking greenhouse gas (GHG) emissions from international shipping as soon as possible, reaching net-zero GHG emissions by or around 2050[59], this percentage will increase. Moreover, this ship-related emission will remain, as it is not addressed by the current emission reduction strategy[59]. Considering the results of this study, a potential mitigation for ship-induced CH_4 emissions, would be smaller and slower vessels, a measure which would also reduce the emission of underwater noise[60], hence give synergistic effects in reducing the environmental impact from shipping.

Our observations reinforce the challenge of assessing the large spatiotemporal variation of CH_4 emissions, and the importance of understanding the governing processes when planning field observations. Generally, shipping lanes and intensely trafficked areas are avoided during field observations. As shipping lanes are potential local CH_4 emission hotspots, they should be included when estimating natural emission/flux from coastal and estuarine areas. Moreover, the process of ship-triggered gas flux in estuarine areas is not only affecting CH_4 but could also affect emissions of other GHGs in the water column, such as nitrous oxide (N_2O) and CO_2. As N_2O has an even higher global warming potential than CH_4, and is known to be produced in estuarine hypoxic areas[46], it would be relevant to include N_2O emissions in future estimates of ship-triggered GHG emissions from shipping lanes.

As a majority of the world's largest ports[44] are located in waters with CH_4 rich sediments[23,24,45,46] (Supplementary Table 1), the contribution of ship-induced CH_4 emissions have global implications, and needs further investigation. Hence, future studies should include in situ measurements of the below-ship pressure, sediment CH_4 flux, and CH_4 concentrations in the water, to better resolve the correlation between the ship-induced pressure change and CH_4 emission magnitude and occurrence. To conclude, we have shown that ships do not only emit greenhouse gasses through fuel consumption but can also trigger significant CH_4 emissions from natural source and, most importantly, that these emissions are frequently overlooked due to a lack of sampling in shipping lanes.

Methods

Field campaign

During two field campaigns from August 25 to September 4, 2011, and from June 27 to July 4, 2012, shipborne observations of ship plumes (NO_x, SO_2, CO_2 and CH_4) were carried out in the Neva Bay (Fig. 2 for illustration of field work setup). A detailed description of the campaigns has previously been published[39], except for the CH_4 measurements described in this work.

The inlet channel to Saint Petersburg in Neva Bay (Fig. 1), was the site of ship measurements conducted during this study. Neva Bay is a shallow estuarine lagoon located at the mouth of the Neva River, which is closed off from the Gulf of Finland by a flood protective dam[61] (Fig. 1). The ship traffic is limited to two designated vessel gates, with the 200 m wide main vessel gate located just south of the Kotlin island[61,62]. The general water depth in the bay is 2–5 m, but between the main vessel gate and Saint Petersburg port there is a dredged navigation channel which is approximately 14 m deep, 120 m wide, and 27.3 km long (Wärtsilä NaviPlanner Tool, Electronic Navigational Chart) (Fig. 2). The sediment in the dredged channel and large part of the area surrounding the channel, is silty-clay mud[61,63]. The estuary is well mixed with a low salinity (0.07–0.2 psu) and occasional intrusion of brackish water during surge events[57]. The Neva Bay is eutrophic, with a large input of organic matter[57] and high water CH_4 concentrations have been observed (mean 95 nmol L^{-1})[43]. The average water discharge from the Neva River is 2490 m^3 s^{-1} [64] with an estimated riverine CH_4 of 0.25 mol s^{-1} [43]. The shallow water depth, large riverine input of organic matter, dam structure, and low salinity of the Neva Bay[65], provide ideal conditions for biogenic production of CH_4 in the sediment[4,14,56].

Field observation instrumentation

The primary instrument used in the study was a Picarro CRDS (cavity ring-down spectrometer) model G2304. This instrument sequentially measures CO_2, H_2O, and CH_4 values with a sampling frequency of 1 Hz, with each species being measured for approximately 0.3 s. The detection limits (3σ) for CO_2 and CH_4 are 200 ppb and 1 ppb, respectively. The CRDS was connected to an inlet at a height of 5 m through a 6 mm Teflon tube. For water-air flux measurements, a floating flux chamber was used, consisting of a plastic tube with a height of approximately 200 mm and a diameter of 130 mm. The chamber was connected to the CRDS by circulating air through it using an external pump. The flux chamber required still water to give accurate measurements, thus could not be used in the wind-exposed shipping lane and was therefore deployed in a sheltered part of the Neva River mouth (Fig. 1).

To measure the speed and direction of the wind, a sonic wind metre (Airmar 200WX-IPX7) was used, which transmits ultrasonic waves between its two sensor heads. Automatic Identification System (AIS) data for the observed ships were logged and used to obtain vessel specific information about ship speed. In addition to gas measurements, water sampling was conducted at different depths to measure oxygen levels, salinity, and temperature using a Sea-Bird SBE19plus (Sea-Bird Electronics, Inc.) CTD (conductivity, temperature, depth).

CH_4 emission and flux calculation

The CRDS measures the volume mixing ratio [x] of a certain gas and for each detected plume a time integrated value (x_{Area}), was calculated according to (Eq. 1):

$$x_{\mathrm{Area}} = \int_{\text{plume start}}^{\text{plume end}} \Big([x] - [x_{\mathrm{Background}}] \Big) \mathrm{d}t \tag{1}$$

where [$x_{Background}$] is the background volume mixing ratio on either side of the plume (Supplementary Fig. 5). A typical measurement of a by-passing ship is shown in Supplementary Fig. 2, for both CO_2 and CH_4, and here the distinct time lag between the two plumes should be noted. This clearly shows that the plumes have different origin, i.e. ship exhaust and the wake water behind the ship. More details of the area calculation of the plume are shown in Supplementary Fig. 5. An in-house developed software (IGPS)[46] was used to identify CO_2 and CH_4 plumes in the CRDS observations and match the plumes with ships in the AIS data. The instrument position, ship position, and timestamps at the beginning and end for each analysed plume are noted in Supplementary Data 1. The IGPS software was also used to calculate x_{Area}, max peak height, and the average and standard deviation of [$x_{Background}$](Supplementary Fig. 5).

To calculate the CH_4 emission [g s^{-1}], denoted E_{CH_4}, the ratio of the measured time integrated areas of CH_4 and CO_2 was multiplied with the modelled fuel consumption [g_{CO_2} s^{-1}] for each ship at the observed speed, obtained using the Ship Traffic Emission Assessment Model (STEAM) model[41], as expressed in Eq. (2):

$$E_{\mathrm{CH_4}} = Q_{\mathrm{CO_2}} \cdot \frac{\int_{\text{plume start}}^{\text{plume end}} \Big([CH_4] - [CH_{4\,\mathrm{Background}}] \Big) \mathrm{d}t \times M_{\mathrm{CH_4}}}{\int_{\text{plume start}}^{\text{plume end}} \Big([CO_2] - [CO_{2\,\mathrm{Background}}] \Big) \mathrm{d}t \times M_{\mathrm{CO_2}}} \tag{2}$$

Where E_{CH_4} is CH_4 emission [g s^{-1}], Q_{CO_2} is modelled CO_2 emission [g s^{-1}] and the integrals correspond to the plume areas (x_{Area}) from the measurements. A CH_4 molar mass (M_{CH_4}) of 16.04 g mol^{-1} and a CO_2 molar mass (M_{CO_2}) of 44.01 g mol^{-1}, was used.

This approach is similar to the one used for remote measurements of emission factors of NO_x and SO_2 [$g_{pollutant}/kg_{fuel}$][39]. It should be noted that it is assumed that CO_2 and CH_4 disperse in the same manner in height, despite their different origins. This assumes that these measurements are conducted far enough away from the ships (>1000 m) to allow for a homogeneous mixing in the lower atmosphere. The dispersion error associated with this assumption was estimated to be lower than 60%, unless the vessel is large and passing very close to the instrument (full discussion on dispersion error estimate available in the Supplementary Methods and Supplementary Fig. 6). A dispersion error parameter was not included in the emission uncertainty estimate (see Supplementary Methods for uncertainty estimate calculation), as information about the ship wind wake effect was not available.

The ship-induced CH_4 emissions in Neva Bay were calculated for a 5.46 km long area in the dredged shipping lane channel (120 m wide) where the measurements were generally carried out (Fig. 1). The total CH_4 emission per ship passage was calculated by multiplying the CH_4 emission rate for each ship with the time the ship spent in the shipping lane, based on its speed. To be included in the CH_4 emission calculation, a plume had to meet four criteria: (1) have a significant CO_2 plume; a CO_2 plume was considered as significant if the average volume mixing ratio (VMR) of CO_2 was greater

than three times the standard deviation of the CO_2 background level on both sides of the plume, and the area of the plume was greater than 20 ppm·s., (2) match with a single ship in the AIS database; co-occurring ship passages disabled assignment of the observed ship induced CH_4 emission to a single ship, (3) have a complete observation which was free from interruptions by instrument calibrations, and (4) originate from a ship present in the STEAM ship database. For CH_4 emissions, the categorization of a significant plume (denoted clear CH_4 emission) was more conservative than for the CO_2 plume, with an average VMR of CH_4 greater than four times the standard deviation of the CH_4 background level. The total daily ship-induced CH_4 emission in the studied area was calculated by summing all the ship-induced CH_4 emissions from a 24-h measurement period (14:26:46 August 30 to 14:33:14 August 31, 2011). Observations fulfilling the four requirements for inclusion in the CH4 emission dataset, were used directly in the total daily emission calculation. Three observations had clear CH_4 emissions, but lacked a clear CO_2 plume, a clear ship match, or was not present in the STEAM database, and for those passages the ship type median CH_4 emission was used in the daily emission calculation instead of the ship-specific emission (Table 1). The total daily ship-induced CH_4 flux (F_{SL}) (mmol m^{-2} day^{-1}) in the sampled area of the shipping lane, was calculated by dividing the total daily ship-induced CH_4 emission with the sampled section area (0.66 km^2).

Frequency dataset

The daily CH_4 flux in the shipping lane was estimated by dividing the total daily ship induced CH_4 emission by the area of the ship channel in the sampled section. However, since the CH_4 emission dataset only included 47% of all the detected plumes, it was not suitable for estimating the CH_4 emission frequency. Therefore, an additional CH_4 emission frequency dataset was created, containing observations from five of the sampling days, selected for their high volume of ship passages and favourable sampling conditions. All detected emissions, except those observed during movement and calibrations, were included in the frequency dataset. Nevertheless, a large portion of the frequency dataset either lacked the AIS-data (6%), and no ship was allocated to the emission, or a significant CO_2 plume was lacking (32%). Thus, the CH_4 emission rates could not be obtained directly using Eq. (2). The CH_4 emission can also be calculated if the dilution of the observed plume is known, however, accurately calculating a dilution factor for each observed plume was outside the scope of this study. Nevertheless, as the dilution is related to the wind speed, we calculated an emission proxy (E_{proxy}) using the observed mixing ratio area x_{Area} [ppm s] from Eq. (1) and the wind speed U_{wind} [m s^{-1}], according to Eq. (3):

$$E_{proxy} = x_{Area} \cdot U_{wind} \tag{3}$$

E_{proxy} thus represents the magnitude of the observed emission corrected for wind speed (with the arbitrary unit [ppm m]), which provides an emission estimate which can be used to compare the relative magnitude of the ship-triggered emissions between passages. The emission proxy clearly correlated with the calculated CH_4 emissions ($R^2 = 0.8553$) (Supplementary Fig. 7) and was considered suitable to estimate emission frequency and indicate the relative magnitude between emissions (see Supplementary Methods for details).

All vessel information was retrieved from the Sea-web Ships[66] database. The uncertainty was calculated following the GUM (Guide to the Expression of Uncertainty in Measurement) ISO/IEC Guide 98-3:2008[67] (details in Supplementary Methods).

Ship-induced pressure change calculation

According to Bernoulli's principle, assuming negligible energy loss, the decrease in pressure under the ship is proportional to the increase in square of the water speed in a frame of reference following the ship. Here, the change in pressure (ΔP) has been estimated according to Eq. (4):

$$\frac{\rho}{2}\left(U_s^2 - U_0^2\right) = -\Delta P \tag{4}$$

where U_0 is the ship speed, which represents the upstream undisturbed flow towards the ship in a frame of reference following the ship, U_s is the water speed under the ship [m s^{-1}], also relative to the ship, ρ is the water density [kg m^{-3}] ($\sim$1000 kg m^{-3}, Supplementary Fig. 3), and -ΔP is the change in pressure [Pa]. In a frame of reference following the ship, the water flowing towards the ship needs to accelerate to keep the mass flux constant past the obstacle. The amount of acceleration depends on the cross-sectional area around the ship that is influence by its presence. If the width that is influenced is w_0, the average velocity inside this area and outside the ship can be calculated from continuity according to Eq. (5), to be

$$U_s = U_0 \cdot \frac{w_0 \times h}{(w_0 \times h - w_s \times D)} \tag{5}$$

where w_0 is the width of the influenced area, w_s is the width [m] of the ship, h is the channel water depth (14 m), and D is the ship draught [m]. This is a lower estimate of the magnitude of the pressure drop, since it is assumed that the water accelerates uniformly around the ship in the whole cross-section, whereas, in reality, the acceleration, and thereby the pressure drop, is larger close to, and below the ship.

Relative contribution of ship-triggered CH_4 emissions

The relative contribution of the ship-triggered CH_4 emissions in the shipping lane ($E_{CH_4,SL}$) compared to the total Neva Bay CH_4 emission, was estimated according to Eq. (6):

$$\text{Quota}_{E_{CH_4},SL} = \frac{F_{SL} \cdot A_{SL}}{(F_{NB} \cdot (A_{tot} - A_{SL}) + F_{SL} \cdot A_{SL})} \tag{6}$$

Where F_{SL} is the daily shipping lane flux, A_{SL} is the shipping lane area (27.3 km · 120 m), F_{NB} is the ambient daily flux in the Neva Bay, and A_{NB} is the Neva Bay area calculated as the total Neva Bay area (A_{tot}) minus the shipping lane area (A_{SL}).

CFD modelling of ship-induced pressure and turbulence

To complement the field measurements, CFD simulations were performed of two different ships in the environment studied. The objectives were to get detailed information on the pressure field imposed by the ship and the mixing incurred by the fluid motions caused by the propeller in the ship wake. Detailed ship data were not available for any of the observed vessel, such as hull design, draft, propulsion arrangement, or shaft rpm. Thus, two generic ship models were selected as representative vessels for ship types with different emission characteristics in the field observations, one single screw tanker and one twin screw RoPax. The tanker had a waterline length of 96.7 m, beam of 15.4 m, draught of 6.0 m, and a speed of 10 knots. The RoPax had a waterline length of 172.1 m, beam 14.4 m, draught 6.8 m, and speed 12 knots. The tanker geometry was similar to the vessels not inducing clear CH_4 emissions in the large tanker category (Supplementary Data 1), and the RoPax vessel was similar to the RoPax vessels in the dataset, which often induced clear CH_4 emissions. The sea floor bathymetry was created to mimic the water depth (14 m) and width (120 m) of the shipping lane, with the depth outside the lane being 4 m (Figs. 2, 6); the full area simulated was 700 × 550 m.

The ships were simulated in full-scale using DDES (Delayed Detached Eddy Simulation) modelling and the k-ω-SST turbulence model with wall functions[68]. The open source libraries of OpenFOAM were used to perform the simulations[69]. In order to capture the turbulence generated by the propeller and the induced rotational effects on the ship wake, resolved rotating propellers were used in combination with a refinement box stretching aft of the ship for several ship lengths. However, to save computational effort, the ship generated waves were not resolved. At the ship speeds in question, waves are small and are not expected to contribute substantially to the pressure field on the sea floor. Mesh sizes were 22 M cells for the tanker and 42 M cells for the RoPax. Cell sizes around the propeller were below 2 mm transitioning to 10 cm in the wake region. Simulations

were run for more than 30 s real time with a time step corresponding to less than 0.05° of propeller revolution.

Statistical analysis

The relationship between CH_4 emissions and ship characteristics, including length, draught, speed, and pressure variations, was investigated using a mixture modelling approach. This method integrated a logistic regression model to differentiate between the presence or absence of clear CH_4 emissions, and a log-normal regression model to estimate CH_4 emission concentrations when emissions were detected. The equation for the fitted curve followed the form in Eq. (7):

$$y = \frac{1}{1 + e^{a-bx}} \cdot e^{c+dx}, \tag{7}$$

where the first term represents the logistic function, the second term represents the log-normal regression function, x is the value of the explanatory ship-related variable (e.g. pressure change), and a, b, c, and d are parameters estimated from the data. Odds ratios (ORs) from the logistic regression model were used to quantify the likelihood of clear CH_4 emissions relative to no emissions per specified unit increase (20 mbar pressure, 1 m ship draught, 50 m ship length, and 1 knot speed) in the explanatory variables. Additionally, log-linear quasi-Poisson regression was employed to estimate fold changes in CH_4 emissions per specified unit of increase in these variables. Analyses were performed using SAS Enterprise Guide 8.4.

The correlation between CH_4 emission magnitude and temperature and air pressure, was estimated as the R^2 value from a linear regression fitted to the clear CH_4 emissions in the frequency dataset versus air pressure/temperature measurements from the St Petersburg station in the International Surface Pressure Databank version 4[70]. The correlation between emission frequency and air pressure/temperature was tested using a single factor analysis of variance (ANOVA) (alpha 0.05), with the null hypothesis that the mean air pressure/temperature in the clear CH_4 emissions group (frequency dataset) was not statistically significantly different from the mean air pressure/temperature in the no clear CH_4 emissions group (frequency dataset).

Data availability

The authors declare that the data supporting the findings of this study are available within the paper, its Supplementary Information files, and in Zenodo with the identifier https://doi.org/10.5281/zenodo.15313158[71], and the International Surface Pressure Databank version 4 (https://doi.org/10.5065/9EYR-TY90)[70]. Should any raw data files be needed in another format they are available from the corresponding author upon reasonable request. The AIS data and technical description of the world fleet used as input to STEAM are governed by contracts with third parties and cannot be shared, but these data are openly available for purchase from their providers.

Code availability

The IGPS software and its source code is the property of Chalmers University of technology and is not available for people outside Chalmers. All calculations performed using the IGPS software are described within the paper. STEAM and its source code are property of the Finnish Meteorological Institute (FMI) and are not available.

Received: 13 September 2024; Accepted: 2 May 2025;
Published online: 15 May 2025

References

1. Saunois, M. et al. The global methane budget 2000–2017. *Earth Syst. Sci. Data* **12**, 1561–1623 (2020).
2. IPCC. In *Climate Change 2022: Mitigation of Climate Change. Contribution of Working Group III to the Sixth Assessment Report of the Intergovernmental Panel on Climate Change* (eds P. R. Shukla et al.), (Cambridge University Press, 2022).
3. Rosentreter, J. A. et al. Half of global methane emissions come from highly variable aquatic ecosystem sources. *Nat. Geosci.* **14**, 225–230 (2021).
4. Wallenius, A. J., Dalcin Martins, P., Slomp, C. P. & Jetten, M. S. Anthropogenic and environmental constraints on the microbial methane cycle in coastal sediments. *Front. Microbiol.* **12**, 631621 (2021).
5. Weber, T., Wiseman, N. A. & Kock, A. Global ocean methane emissions dominated by shallow coastal waters. *Nat. Commun.* **10**, 4584 (2019).
6. Corbett, J. J., Fischbeck, P. S. & Pandis, S. N. Global nitrogen and sulfur inventories for oceangoing ships. *J. Geophys. Res. Atmos.* **104**, 3457–3470 (1999).
7. Fu, M., Liu, H., Jin, X. & He, K. National- to port-level inventories of shipping emissions in China. *Environ. Res. Lett.* **12**, 114024 (2017).
8. Grönholm, T. et al. Evaluation of Methane Emissions Originating from LNG Ships Based on the Measurements at a Remote Marine Station. *Environ. Sci. Technol.* **55**, 13677–13686 (2021).
9. Faber, J. et al. Reduction of GHG emissions from ships—Fourth IMO GHG study 2020—Final report. *IMO MEPC* **75**, 15 (2020).
10. Balcombe, P., Heggo, D. A. & Harrison, M. Total Methane and CO2 Emissions from Liquefied Natural Gas Carrier Ships: The First Primary Measurements. *Environ. Sci. Technol.* **56**, 9632–9640 (2022).
11. Hofmann, H., Federwisch, L. & Peeters, F. Wave-induced release of methane: Littoral zones as source of methane in lakes. *Limnol. Oceanogr.* **55**, 1990–2000 (2010).
12. Maeck, A., Hofmann, H. & Lorke, A. Pumping methane out of aquatic sediments–ebullition forcing mechanisms in an impounded river. *Biogeosciences* **11**, 2925–2938 (2014).
13. Lohrberg, A. et al. Discovery and quantification of a widespread methane ebullition event in a coastal inlet (Baltic Sea) using a novel sonar strategy. *Sci. Rep.* **10**, 4393 (2020).
14. Humborg, C. et al. High emissions of carbon dioxide and methane from the coastal Baltic Sea at the end of a summer heat wave. *Front. Mar. Sci.* **6**, 493 (2019).
15. Römer, M., Riedel, M., Scherwath, M., Heesemann, M. & Spence, G. D. Tidally controlled gas bubble emissions: A comprehensive study using long-term monitoring data from the NEPTUNE cabled observatory offshore Vancouver Island. *Geochem. Geophys. Geosyst.* **17**, 3797–3814 (2016).
16. Thornton, B. F. et al. Shipborne eddy covariance observations of methane fluxes constrain Arctic sea emissions. *Sci. Adv.* **6**, eaay7934 (2020).
17. Schubert, C. J., Diem, T. & Eugster, W. Methane emissions from a small wind shielded lake determined by Eddy covariance, flux chambers, anchored funnels, and boundary model calculations: A comparison. *Environ. Sci. Technol.* **46**, 4515–4522 (2012).
18. Lundevall-Zara, M., Lundevall-Zara, E. & Brüchert, V. Sea-air exchange of methane in shallow inshore areas of the Baltic Sea. *Front. Mar. Sci.* **8**, 657459 (2021).
19. Fredriksson, S. T., Arneborg, L., Nilsson, H., Zhang, Q. & Handler, R. A. An evaluation of gas transfer velocity parameterizations during natural convection using DNS. *J. Geophys. Res.-Oceans* **121**, 1400–1423 (2016).
20. Wanninkhof, R., Asher, W. E., Ho, D. T., Sweeney, C. & McGillis, W. R. Advances in quantifying air-sea gas exchange and environmental forcing. *Annu. Rev. Mar. Sci.* **1**, 213–244 (2009).
21. Liang, J.-H. In *Recent* Advances in *the Study of Oceanic Whitecaps: Twixt Wind and Waves* (eds Penny Vlahos & Edward C. Monahan), 107-120 (Springer International Publishing, 2020).
22. Emerson, S. & Bushinsky, S. The role of bubbles during air-sea gas exchange. *J. Geophys. Res. -Oceans* **121**, 4360–4376 (2016).
23. Borges, A. V., Champenois, W., Gypens, N., Delille, B. & Harlay, J. Massive marine methane emissions from near-shore shallow coastal areas. *Sci. Rep.* **6**, 1–8 (2016).

24. Zang, K. et al. Multiple factors dominate the distribution of methane and its sea-to-air flux in the Bohai Sea in summer and autumn of 2014. *Mar. Pollut. Bull.* **154**, 111049 (2020).
25. Bonaglia, S. et al. High methane emissions from an anoxic fjord driven by mixing and oxygenation. *Limnol. Oceanogr. Lett.* **7**, 392–400 (2022).
26. Hermans, M. et al. Ebullition dominates methane emissions in stratified coastal waters. *Sci. Total Environ.* **945**, 174183 (2024).
27. Mattson, M. D. & Likens, G. E. Air pressure and methane fluxes. *Nature* **347**, 718–719 (1990).
28. Wilkinson, J., Maeck, A., Alshboul, Z. & Lorke, A. Continuous seasonal river ebullition measurements linked to sediment methane formation. *Environ. Sci. Technol.* **49**, 13121–13129 (2015).
29. von Deimling, J. S., Greinert, J., Chapman, N. R., Rabbel, W. & Linke, P. Acoustic imaging of natural gas seepage in the North Sea: Sensing bubbles controlled by variable currents. *Limnol. Oceanogr. Methods* **8**, 155–171 (2010).
30. Briggs, M. J., Vantorre, M., Uliczka, K. & Debaillon, P. In *Handbook of Coastal and Ocean Engineering* (ed Young C. Kim), 1029-1080 (World Scientific, 2018).
31. Weber, T. C., Lyons, A. P. & Bradley, D. L. An estimate of the gas transfer rate from oceanic bubbles derived from multibeam sonar observations of a ship wake. *JGRC* **110**, https://doi.org/10.1029/2004JC002666 (2005).
32. Trevorrow, M. V., Vagle, S. & Farmer, D. M. Acoustical measurements of microbubbles within ship wakes. *J. Acoust. Soc. Am.* **95**, 1922–1930 (1994).
33. Nylund, A. T., Arneborg, L., Tengberg, A., Mallast, U. & Hassellöv, I. M. In situ observations of turbulent ship wakes and their spatiotemporal extent. *Ocean Sci.* **17**, 1285–1302 (2021).
34. Nylund, A. T. et al. Hydrographical implications of ship-induced turbulence in stratified waters, studied through field observations and CFD modelling. *Front. Mar. Sci*. **10**, https://doi.org/10.3389/fmars.2023.1273616 (2023).
35. Shakhova, N. et al. Ebullition and storm-induced methane release from the East Siberian Arctic Shelf. *Nat. Geosci.* **7**, 64–70 (2014).
36. Borges, A. V., Speeckaert, G., Champenois, W., Scranton, M. I. & Gypens, N. Productivity and temperature as drivers of seasonal and spatial variations of dissolved methane in the Southern Bight of the North Sea. *Ecosystems* **21**, 583–599 (2018).
37. Shalini, A., Ramesh, R., Purvaja, R. & Barnes, J. Spatial and temporal distribution of methane in an extensive shallow estuary, south India. *J. Earth Syst. Sci.* **115**, 451–460 (2006).
38. Chen, X., Schäfer, K. V. & Slater, L. Methane emission through ebullition from an estuarine mudflat: 2. Field observations and modeling of occurrence probability. *Water Resour. Res*. **53**, 6439–6453 (2017).
39. Beecken, J. et al. Emission factors of SO2, NOx and particles from ships in Neva Bay from ground-based and helicopter-borne measurements and AIS-based modeling. *Atmos. Chem. Phys.* **15**, 5229–5241 (2015).
40. Balzani Lööv, J. M. et al. Field test of available methods to measure remotely SO_x and NO_x emissions from ships. *Atmos. Meas. Tech.* **7**, 2597–2613 (2014).
41. Jalkanen, J.-P. et al. A modelling system for the exhaust emissions of marine traffic and its application in the Baltic Sea area. *Atmos. Chem. Phys.* **9**, 9209–9223 (2009).
42. HELCOM. HELCOM Assessment on maritime activities in the Baltic Sea 2018. Baltic Sea Environment Proceedings No.152. 253 (Helsinki Commission, Helsinki, Finland, 2018).
43. Schneider, B., Gülzow, W., Sadkowiak, B. & Rehder, G. Detecting sinks and sources of CO2 and CH4 by ferrybox-based measurements in the Baltic Sea: Three case studies. *J. Mar. Syst.* **140**, 13–25 (2014).
44. UNCTAD. Review of maritime transport 2022, Navigating stormy waters, UNCTAD/RMT/2022. (United Nations Publications, New York, 2022).
45. Mao, S.-H. et al. Aerobic oxidation of methane significantly reduces global diffusive methane emissions from shallow marine waters. *Nat. Commun.* **13**, 7309 (2022).
46. Liu, S. et al. Spatial distribution and influencing mechanism of CO2, N2O and CH4 in the Pearl River Estuary in summer. *Sci. Total Environ.* **846**, 157381 (2022).
47. Deemer, B. R. et al. Greenhouse gas emissions from reservoir water surfaces: a new global synthesis. *Bioscience* **66**, 949–964 (2016).
48. Maeck, A. et al. Sediment Trapping by Dams Creates Methane Emission Hot Spots. *Environ. Sci. Technol.* **47**, 8130–8137 (2013).
49. Gutiérrez-Loza, L. et al. Measurement of air-sea methane fluxes in the Baltic Sea using the eddy covariance method. *Front. Earth Sci.* **7**, 93 (2019).
50. Myllykangas, J.-P., Hietanen, S. & Jilbert, T. Legacy Effects of Eutrophication on Modern Methane Dynamics in a Boreal Estuary. *Estuaries Coasts* **43**, 189–206 (2020).
51. Bange, H. W., Bartell, U. H., Rapsomanikis, S. & Andreae, M. O. Methane in the Baltic and North Seas and a reassessment of the marine emissions of methane. *Glob. Biogeochem. Cycles* **8**, 465–480 (1994).
52. Gülzow, W. & Rehder, G. Schneider v Deimling, J., Seifert, T. & Tóth, Z. One year of continuous measurements constraining methane emissions from the Baltic Sea to the atmosphere using a ship of opportunity. *Biogeosciences* **10**, 81–99 (2013).
53. Bussmann, I., Brix, H., Flöser, G., Ködel, U. & Fischer, P. Detailed patterns of methane distribution in the German Bight. *Front. Mar. Sci.* **8**, 728308 (2021).
54. Roth, F. et al. High spatiotemporal variability of methane concentrations challenges estimates of emissions across vegetated coastal ecosystems. *Glob. Change Biol.* **28**, 4308–4322 (2022).
55. Middelburg, J. J. et al. Methane distribution in European tidal estuaries. *Biogeochemistry* **59**, 95–119 (2002).
56. Egger, M., Riedinger, N., Mogollón, J. M. & Jørgensen, B. B. Global diffusive fluxes of methane in marine sediments. *Nat. Geosci.* **11**, 421–425 (2018).
57. Golubkov, S., Golubkov, M., Tiunov, A. & Nikulina, V. Long-term changes in primary production and mineralization of organic matter in the Neva Estuary (Baltic Sea). *J. Mar. Syst.* **171**, 73–80 (2017).
58. Forster, P. et al. The Earth's Energy Budget, Climate Feedbacks, and Climate Sensitivity. In *Climate Change 2021: The Physical Science Basis. Contribution of Working Group I to the Sixth Assessment Report of the Intergovernmental Panel on Climate Change* (eds V. Masson-Delmotte et al.), 923–1054 (Cambridge University Press, Cambridge, United Kingdom and New York, NY, USA 2021).
59. MEPC. ANNEX 1 RESOLUTION MEPC.377(80), Adopted on 7 July 2023, 2023 IMO strategy on reduction of GHG emissions from ships. (2023).
60. Merchant, N. D. Underwater noise abatement: Economic factors and policy options. *Environ. Sci. Policy* **92**, 116–123 (2019).
61. Ryabchuk, D. et al. In *The Diversity of Russian Estuaries and Lagoons Exposed to Human Influence* (ed Ruben Kosyan), 191-221 (Springer International Publishing, 2017).
62. Hunter, P. in *CETMEF PIANC Paris 2012* (Paris, 2012).
63. Ryabchuk, D. et al. Coastal erosion processes in the eastern Gulf of Finland and their links with geological and hydrometeorological factors. *Boreal Environ. Res.* **16**, 117–137 (2011).
64. Golubkov, M., Nikulina, V. & Golubkov, S. Species-level associations of phytoplankton with environmental variability in the Neva Estuary (Baltic Sea). *Oceanologia* **63**, 149–162 (2021).

65. Telesh, I. V., Golubkov, S. M. & Alimov, A. F. In *Ecology of Baltic Coastal Waters* (ed Ulrich Schiewer) 259-284 (Springer Berlin Heidelberg, 2008).
66. Sea-web Ships. https://maritime.ihs.com (2022).
67. Joint Committee for Guides in Metrology Evaluation of measurement data—Guide to the expression of uncertainty in measurement. *JCGM* **100**, 1–116 (2008).
68. Gritskevich, M. S., Garbaruk, A. V., Schütze, J. & Menter, F. R. Development of DDES and IDDES formulations for the k-ω shear stress transport model. *Flow. Turbulence Combust.* **88**, 431 (2012).
69. Weller, H. G., Tabor, G., Jasak, H. & Fureby, C. A tensorial approach to computational continuum mechanics using object-oriented techniques. *Comput. Phys.* **12**, 620–631 (1998).
70. Compo, G. P. et al. (Research Data Archive at the National Center for Atmospheric Research, Computational and Information Systems Laboratory, Boulder, CO, 2019).
71. Nylund, A. "Measurements of ship-triggered methane emissions in Neva Bay, Russia in 2011 and 2012". *Zenodo* https://doi.org/10.5281/zenodo.15313158 (2025).

Acknowledgements

This project has received funding from the Swedish Agency for Marine and Water Management [grant agreement No 810-23] and Chalmers Area of Advance Transport. The computations were enabled by resources provided by the National Academic Infrastructure for Supercomputing in Sweden (NAISS) and the Swedish National Infrastructure for Computing (SNIC) at NSC partially funded by the Swedish Research Council through grant agreements no. 2022-06725 and no. 2018-05973 and by resources provided by Chalmers e-Commons at Chalmers. The financial support from the EU H2020 project EMERGE is appreciated, which has received funding from the European Union's Horizon 2020 research and innovation programme under grant agreement no. 874990 (EMERGE project). We would like to thank Reto Weber for assistance with the Electronic Navigational Charts (ENC). The authors would like to acknowledge support from InfraVis for providing application expertise for visualisation through Swedish Research Council grant 2021-00181.

Author contributions

A.T.N. wrote the original draft, participated in the development and design of the methodology, software and code, and conducted the formal analysis and data visualization. J.M. was responsible for the conceptualization of the study and funding acquisition, participated in the development and design of the methodology, software and code, conducted the field work and provided field work resources, conducted the formal analysis, gave input to the data visualization, and edited and reviewed the manuscript draft. V.C. participated in the development and design of the methodology, software and code, conducted the field work and provided field work resources, conducted the formal analysis, gave input to the data visualization, and edited and reviewed the manuscript draft. K.S. participated in the development and design of the methodology, conducted the field work, provided field work resources, and edited and reviewed the manuscript draft. R.B. was responsible for the conceptualization of the study and funding acquisition, participated in the development and design of the methodology, software and code, conducted the CFD modelling, formal analysis and data visualization, provided modelling resources, and edited and reviewed the manuscript draft. L.A. participated in the development and design of the methodology, provided field work resources, conducted the formal analysis, gave input to the data visualization, edited and reviewed the manuscript draft, and supervised A.T.N. J.-P.J. participated in the development and design of the methodology, software and code, provided modelling resources, and edited and reviewed the manuscript draft. A.T. was responsible for the funding acquisition, provided field work resources, edited and reviewed the manuscript draft, and supervised A.T.N. I.-M.H. was responsible for the conceptualization of the study and funding acquisition, participated in the development and design of the methodology, wrote the original draft, gave input to the data visualization, provided field work resources, and supervised A.T.N.

Funding

Open access funding provided by Chalmers University of Technology.

Competing interests

The authors declare no competing interests.

Additional information

Supplementary information The online version contains supplementary material available at https://doi.org/10.1038/s43247-025-02344-8.

Correspondence and requests for materials should be addressed to Amanda T. Nylund or Ida-Maja Hassellöv.

Peer review information *Communications Earth & Environment* thanks Martijn Hermans, Thomas Weber and the other, anonymous, reviewer(s) for their contribution to the peer review of this work. Primary Handling Editor: Alice Drinkwater. [A peer review file is available.